



HAL
open science

Super-resolution in near-field acoustic time reversal using reverberated elastic waves in skull-shaped antenna

Michael Reinwald, Quentin Grimal, Stefan Catheline, Lapo Boschi

► To cite this version:

Michael Reinwald, Quentin Grimal, Stefan Catheline, Lapo Boschi. Super-resolution in near-field acoustic time reversal using reverberated elastic waves in skull-shaped antenna. *Acta Acustica united with Acustica*, 2018, 104 (6), pp.963-969. 10.3813/AAA.919262 . hal-01980152

HAL Id: hal-01980152

<https://hal.sorbonne-universite.fr/hal-01980152>

Submitted on 14 Jan 2019

HAL is a multi-disciplinary open access archive for the deposit and dissemination of scientific research documents, whether they are published or not. The documents may come from teaching and research institutions in France or abroad, or from public or private research centers.

L'archive ouverte pluridisciplinaire **HAL**, est destinée au dépôt et à la diffusion de documents scientifiques de niveau recherche, publiés ou non, émanant des établissements d'enseignement et de recherche français ou étrangers, des laboratoires publics ou privés.

Super-resolution in near-field acoustic time reversal using reverberated elastic waves in skull-shaped antenna

Michael Reinwald¹⁾, Quentin Grimal¹⁾, Stefan Catheline²⁾, Lapo Boschi³⁾

¹⁾ Sorbonne Université, CNRS, INSERM, Laboratoire d'Imagerie Biomédicale, LIB, F-75006, Paris, France. michael.reinwald@upmc.fr

²⁾ LabTAU, INSERM, Centre Léon Bérard, Université Lyon 1, Univ Lyon, F-69003, Lyon, France.

³⁾ Sorbonne Université, CNRS-INSU, Institut des Sciences de la Terre Paris, ISTeP UMR 7193, F-75005, Paris, France.

1 Summary

We investigate the potential of using elastic waves for near-field acoustic time reversal, and in doing so evaluate the possibility of reconstructing sound source positions at below-wavelength distances from a skull-shaped acoustic antenna. Our work is based on a conceptual processing model that translates elastic waves conducted and reverberated in an elastic object into source position, through a time reversal analysis. Signals are recorded by passive sensors glued on a replica of a human skull, measuring solely its mechanical vibrations, and not sensitive to airborne sound. The sound source is placed along the azimuthal and sagittal planes for distances to the skull between 5 and 100 cm. We reconstruct the source position for signals with frequencies in the physiological hearing range with a resolution indirectly proportional to the distance between source and skull across all measurements in the far-field. Measurements in the near-field show -3 dB widths smaller than half a wavelength (super-resolution) with highest resolutions of down to $\lambda/15$ measured in front of the orbital cavities. We infer that these anatomical details give rise to complex features of the skull's Green's function, that in turn enhance resolution in a direction-dependent manner.

1 Introduction

It is well known [1] that anatomy contributes to the task of auditory source localization, as its effects on an acoustic signal, described by the head-related transfer function (HRTF) [37, 21], can be seen as a spectral filter and depend on the location of the signal's source. Human auditory source localization mostly relies on differences in the phase and amplitude of signals perceived by the two ears, as well as "spectral cues", or frequency-dependent effects associated with the shape of the pinnae and, possibly, other features of the body ([34]).

Building on the work of Catheline et al. [7], we ex-

plore here the specific role of elastic waves mediated in a skull-shaped object mimicking bone-conducted sound. While this study does not address the issue of whether and how bone conducted sound is employed by the human auditory (ears/brain) system, our goal is to determine whether these reverberated signals contain specific information about the reconstruction of the position of an auditory source, especially in the near-field. This could be relevant to current efforts in the study of bone conduction sound [36, 35, 31, 25, 32]. Using the principle of acoustic time reversal [16, 18], we convert the signal recorded by two receivers into the spatial coordinates of a source in the horizontal and sagittal plane, and evaluate the resolution with which the source position is thus reconstructed.

Catheline et al. [7] showed via a time reversal experiment with a dry skull that in-skull elastic wave propagation provides information about spatial positioning of a sound source. They found that their time reversal algorithm, using elastic waves alone, received at two or only one recording transducer mimicking the ear, successfully reconstructed the source position(s), for single as well as multiple sources. The spatial resolution of this method was found to decrease with increasing distance between the skull and the sound source. This is in good agreement with the far-field diffraction law, which provides a relationship between the spatial resolution and the distance separating the antenna (skull) from the source. Our objective is to expand the early work of Catheline et al. [7] and Ing et al. [22] to (1) analyze the resolution of the same algorithm for a skull-shaped antenna specifically in the near-field, i.e., the sound source is placed closer than one wavelength to the skull, and (2) to evaluate the directionality of the algorithm, i.e. evaluate changes in resolution with respect to angular position of the sound source.

In this study, we conduct a suite of experiments on a simple setup, equivalent to the setup used in Catheline et al. [7], consisting of two recording transducers glued to a replica human skull. Sound is generated

81 by a small speaker deployed at a variety of distances
 82 and azimuths. Our results show in particular that,
 83 in the near-field, the resolution with which we re-
 84 construct the source position changes as a function
 85 of azimuth with respect to the skull and is clearly
 86 influenced by complex features of the skull such as
 87 the orbital cavities. Furthermore we achieve super-
 88 resolution throughout all angles for sources very close
 89 to the skull.

90 Similarly minded experiment have been conducted
 91 in recent years e.g. in the context of optics, where
 92 imaging with evanescent waves allows to surpass the
 93 classical diffraction limit; the super-resolution of near-
 94 field microscopes is piloted by their probe size [28, 24].
 95 In this context, a source [20, 12, 4] or scatterers [14]
 96 smaller than a wavelength, placed within the medium
 97 can be detected in the far-field with super-resolution
 98 as well. Time reversal experiments can also surpass
 99 the diffraction limit when resonators are placed near
 100 a source [23, 29] or when an acoustic sink is used
 101 [9]. To a lesser degree, near-field details can some-
 102 times be extracted from the far-field using sophis-
 103 ticated algorithms such as inverse filter [8] or MU-
 104 SIC [30]. Experiments with metamaterials, super-
 105 lenses and hyper-lenses [27] demonstrate moderate
 106 sub-diffraction imaging down to a quarter of the op-
 107 tical wavelength. All these techniques use different
 108 terminology but they all require some near-field mea-
 109 surements.

110 Because very few studies in psychoacoustics have
 111 explored human sound localization performances for
 112 nearby sources [26], we are unable to determine
 113 whether the resolution achieved by our algorithm re-
 114 produces the performance of human listeners using
 115 bone conducted sound. While we do find that elastic
 116 waves contain sufficient information to successfully re-
 117 construct source positions in the near-field, we cannot
 118 yet establish whether a similar capability is achieved
 119 by the human auditory system.

120 2 Methods

121 The experimental setup is based on the previously
 122 conducted experiment of Catheline et al. [7]: We
 123 use a skull-shaped object (for simplicity from now on
 124 called skull) made of the epoxy resin. The skull is
 125 mounted on a rotatable rod with a reference (hori-
 126 zontal) plane chosen approximately as a plane passing
 127 through the area of the ethmoid bone above the vomer
 128 and through the zygomatic arch and process of the
 129 temporal bone. A conventional loudspeaker (RS Pro
 130 TRG040008) is deployed sequentially at a discrete set
 131 of positions in the horizontal and vertical plane. The
 132 loudspeaker shows a flat frequency response between
 133 200 Hz and 8 kHz. The distance between the source
 134 (loudspeaker) and the skull (the point on the surface
 135 of the skull closest to the speaker), denoted D , varies

136 from 5 to 100 cm, while the source position at each dis-
 137 tance varies with angle φ between -50° (i.e. down,left)
 138 and $+50^\circ$ (i.e. up, right). The experiment is con-
 139 ducted in an anechoic chamber. Equipment which
 140 could possibly reflect sound is covered with multiple
 layers of sound dampening material. Two passive sen-

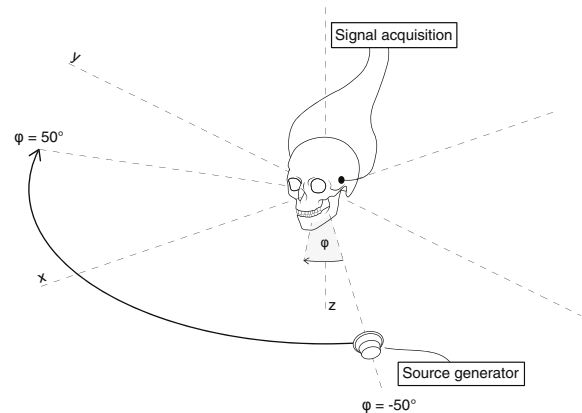


Figure 1: Sketch of the experimental setup in the horizontal plane: A loudspeaker is connected to a source generator (PC) and emits a chirp signal at each angle φ ranging from -50° to 50° along a half circle at various distances to the skull. The resulting vibration of the skull is recorded through two passive sensors glued to the hypothetical ear locations. They are connected to the signal acquisition system, consisting of a sound card connected to a PC.

141 sors (Murata PKS1-4A), with a working bandwidth
 142 ranging between 100 Hz and 15 kHz and a diameter
 143 of 1 cm, are glued close to the hypothetical ear lo-
 144 cations on both sides of the skull. They are used as
 145 receivers to record the elastic vibrations and are con-
 146 nected to a sound card (Soundscape SS8IO-3) which
 147 has a 140 dB dynamic range and a 44.1 kHz sampling
 148 frequency.

A sketch of the experimental setup in the horizontal plane is shown in Figure 1.

152 We checked that the sensors solely measure the vi-
 153 bration of the skull and are unresponsive to airborne
 154 sound. This ensures that the time reversal algorithm
 155 will utilize only elastic waves. Additionally, the in-
 156 fluence of the foam platform used to place the loud-
 157 speaker at certain distances has been tested to have
 158 no influence on sound emission of the loudspeaker.

The first part of the experiment consists of recording the signals at the sensors for each speaker position. The speaker emits a chirp signal $c(t)$ with a duration of 1 s and a linear frequency distribution between 0 Hz and 6 kHz. The function in time for such a chirp of duration T , minimum frequency f_0 and maximum frequency f_1 reads

$$c(t) = \sin \left[\Phi_0 + 2\pi \left(f_0 t + \frac{k}{2} t^2 \right) \right], \quad (1)$$

with the initial phase Φ_0 at time $t = 0$ and the chirpy-

ness $k = \frac{f_1 - f_0}{T}$ (in our case $k = 6000 \text{ Hz/s}$), also
 known as the rate of frequency range across the chirp.
 For each distance D the source positions in the hori-
 zontal plane are defined by the azimuth φ .

The recorded signal s at one of the sensors' location
 r , writes

$$s(\varphi_0, r, t) = c(t) * G(\varphi_0, r, t), \quad (2)$$

where $*$ denotes convolution, φ_0 is the source position
 (azimuth) and $G(\varphi_0, r, t)$ is the acoustic impulse re-
 sponse of the skull, which is also the Green's function
 of the signal emitted at φ_0 and recorded at r , assum-
 ing without loss of generality that emitter and receiver
 are punctual. A representative waveform of a signal
 recorded with one of the sensors and its normalized
 frequency spectrum is shown in Figure 2. Note that

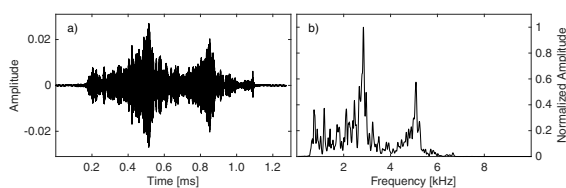


Figure 2: a) Exemplary waveform of a recorded signal
 at one of the sensors. b) Frequency spectrum of the
 same signal.

the spectra of all impulse responses (only one shown
 here) show strong similarity to the results from Cath-
 eline et al. [7] where a real dry skull was used and
 its resonance frequencies were confirmed with other
 studies of dry skulls and cadaver heads [32, 19]. This
 proves that, in the first approximation and for the
 purposes of our study, the epoxy skull replica em-
 ployed here is sufficiently similar to a real skull. It
 should be noted that, firstly, epoxy can have mechani-
 cal properties similar to those of bone tissue ([2, 3]);
 secondly, the most important role in our experiments
 is presumably played by the outer shape of the skull,
 driving wave propagation in air around the skull: and
 the replica is designed to have realistic external shape.

Following Fink [17], the received signal $s(\varphi_0, r, -t)$
 is time-reversed, i.e. flipped with respect to time. It
 must then be backward propagated to any possible lo-
 cation φ_i . This is equivalent to convolving $s(\varphi_0, r, -t)$
 with the Green's function $G(\varphi_i, r, t)$. Since we do not
 have access to $G(\varphi_i, r, t)$, but we do have a library of
 recordings of $s(\varphi_i, r, t)$ for all possible values of φ_i , we
 implement

$$\begin{aligned} T_i(\varphi_0, r, t) &= s(\varphi_0, r, -t) * s(\varphi_i, r, t) = \\ &= c(-t) * G(\varphi_0, r, -t) * c(t) * G(\varphi_i, r, t). \end{aligned} \quad (3)$$

The term $G(\varphi_0, r, t) * G(\varphi_i, r, -t)$ is the transfer func-
 tion of such a time reversal algorithm and, in terms
 of signal analysis, represents a matched filter [17].
 This convolution coincides with the cross-correlation

of $G(\varphi_0, r, t)$ and $G(\varphi_i, r, t)$ ([13, 11]). For each source
 position φ_0 , the signal processing procedure consists
 of implementing Equation 3, i.e. analytically cross-
 correlating the signals, and of finding the maximum
 value, with respect to time, of the time-reversed wave
 field T_i for each φ_i . The resulting function $F(\varphi_i)$
 is dubbed "spatial focusing function" (shortly, focus-
 ing function), as this procedure is equivalent to eval-
 uating whether (and with what resolution) the time-
 reversed and backward-propagated wave field is able
 to reconstruct the original source position φ_0 . The
 focusing function is next normalized with respect to
 its maximum; It is then reasonable to assume that,
 the closer $F(\varphi_i)$ is to 1 (i.e., identical Green's func-
 tions) for a given value of φ_i , the closer φ_i is to
 the original source φ_0 . This method can be interpreted
 as a pattern recognition system, that identifies, from an
 acoustic reference library, the Green's function corre-
 sponding to the actual position of the source, and so
 determines the position of the source.

The invariance under time reversal is lost if the
 propagation medium has frequency-dependent atten-
 uation. This introduces a first-order time derivative
 in the governing propagation equation. However, the
 theorem of spatial reciprocity is still valid, i.e. there
 is a loss of amplitude in the time-reversed vs. for-
 ward propagating wave field, but this does not affect
 source-localization resolution (does not affect the lo-
 cation of the focus of the time-reversed wave field)

We take both sensors into account by computing
 the mean of the focusing functions of the two signals.

In order to investigate the role of different frequency
 contents, the originally measured signals are succes-
 sively filtered with varying low-pass filters with max-
 imum frequency f_{max} .

Following e.g. [22, 5, 33], we estimate the spatial
 resolution of our time reversal algorithm by analyzing
 the -3 dB width Δp of $F(\varphi_i)$ for each given source po-
 sition (angle φ and distance D between the source po-
 sition and the skull) and various smallest wavelengths
 $\lambda_{min} = c/f_{max}$ (with c = speed of sound in air).

We compare our resolution estimates against the
 apparent aperture A of our skull-shaped antenna, as
 defined by Catheline et al. [7], through the far-field
 diffraction law

$$A = \frac{D \cdot \lambda_{min}}{2\Delta p}. \quad (4)$$

While resolution as defined here is known to follow
 the diffraction-law in the far-field [7], that is not the
 case in the near-field, where Equation 4 is only used
 here for the sake of comparison.

3 Results

3.1 Verification of diffraction law

In this section, we reproduce the results of Catheline et al. [7] and verify that our far-field data are consistent with the diffraction law (Equation 4). The source position is chosen to be at $\varphi = 0^\circ$, which is in front of the center of the skull. We calculate the normalized focusing function $F(\varphi_i)$ along the curvilinear abscissa in the horizontal plane as described previously, for each distance to the skull. This is shown in Figure 3

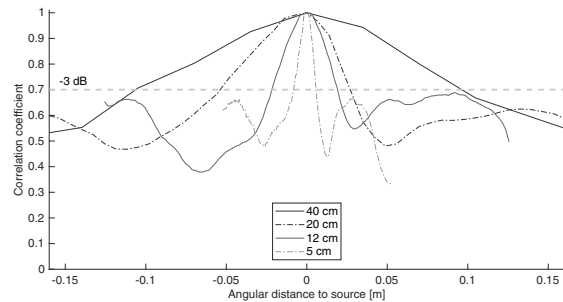


Figure 3: Normalized focusing functions along the curvilinear abscissa for sources in front of the center of the skull ($\varphi = 0^\circ$) and at different distances to the skull. The distance of the measurement points to the skull decreases from 40 cm, down to 20 cm, 12 cm and 5 cm (different curves). There is a clear trend of increasing resolution (decreasing -3 dB width of the curves) with decreasing distance.

as a function of the curvilinear abscissa. The -3 dB (correlation coefficient of 0.7) widths of the curves are in good agreement with the diffraction law, confirming the findings of Catheline et al. [7], where the width of the curve is directly proportional to the distance between skull and sound source. Additionally it can be seen that the maximum peak to ground level (frequently named contrast) of our time reversal scheme lies below -3 dB. This has been confirmed for all measurements and ensures that calculating the resolution is not hindered by a low-contrast focusing function. Figure 4 shows the -3 dB widths of the focusing functions of the signals for sources with different maximum frequencies f_{max} and at different distances in front of the skull ($\varphi = 0^\circ$). We calculate the values of A using Equation 4 and the values shown in Figure 4. They are found to be approximately 10 cm for all distances and maximum frequencies proving that the apparent aperture in the far-field is independent of distance or maximum frequency.

Measurements in the sagittal plane (not shown here) show smaller slopes of the linear fits evaluated in the same way as in Figure 4 across all results. Compared to the case of the horizontal plane, therefore the apparent aperture size is larger for these measurements (15 cm). This may be related to the different

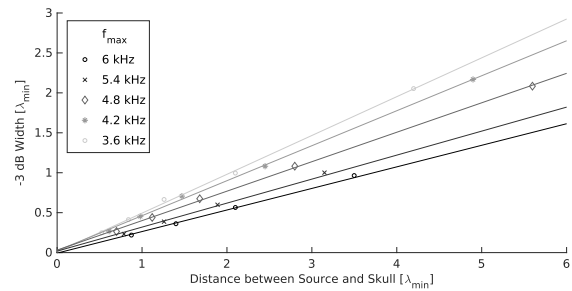


Figure 4: -3 dB width values of the focusing functions for sources at different distances to the skull (x-axis) and maximum frequencies f_{max} of the signal. The slope of each linear fit, which corresponds to the apparent aperture A in Equation 4, is approximately 10 cm for all curves.

diameters of the skull, close to 10 and 15 cm, in the horizontal and sagittal planes, respectively.

The measurement points in the near-field (at distances smaller than one wavelength) lie on the same linear fit (i.e. same apparent aperture) as the points for measurements in the far-field although Equation 4 does not hold true in the near-field. In the near-field, i.e. for sources closer than one minimum wavelength away from the skull, source positions can still be resolved with the same angular resolution which results in super-resolution in space, i.e. -3 dB widths below $0.5 \lambda_{min}$ (see Figure 4). While one could infer that the diffraction limit also holds true in the near-field, our results are purely empirical; any values below the previously formulated diffraction limit are not represented in Equation 4. We speculate that they can be ascribed to the near-field contribution of evanescent waves.

Our far-field data is in agreement with Equation 4 and the previous findings of Catheline et al. [7]. In addition, we are able to achieve the same angular resolution as stated in the far-field diffraction law in the near-field (sound sources at below-wavelength distances) leading to super-resolution.

3.2 Directional variation in resolution

We furthermore investigate the directional variation of resolution of the time reversal analysis in the horizontal plane. The angular variations in resolution of our time reversal scheme in the near-field are visualized in Figure 5 showing the values of A (top) and Δp (bottom) with respect to the source azimuth φ for different source distances (5 cm, 12 cm and 20 cm and 100 cm). All data is filtered to have a maximum frequency of 3 kHz. The reason for an offset of around $2 - 3^\circ$ to the center ($\varphi = 0^\circ$) is due to a limited accuracy in the manual placement of the center position and the center of the rotation axis.

In the far-field, the apparent aperture does not vary with azimuth (see 100 cm data in Figure 5) and is

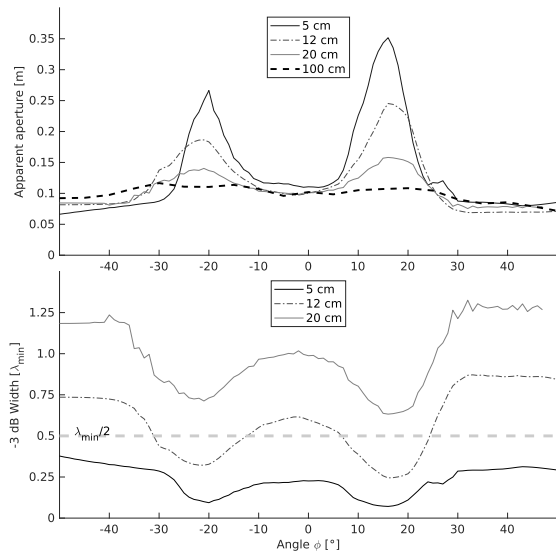


Figure 5: Angular variations of resolution for different source distances. Top: Variation in apparent aperture for different source distances. Maxima are at -20° and 15° whereas the values decrease for source positions close to the center and further away from the center. Bottom: Variation in -3 dB widths for different source distances. Super-resolution is accomplished throughout all angles at a distance of 5 cm and for certain angles at a distance of 12 cm. Highest resolution (smallest -3 dB width) is accomplished for source positions directly in front of the orbital cavities. This effect is (relatively) enhanced the closer the source to the skull.

314 equal to the value of 10 cm obtained from Figure 4
 315 throughout all far-field measurements at source az-
 316 imuth $\varphi = 0^\circ$.

317 In the near-field, the largest apparent aperture val-
 318 ues lie roughly in front of the two orbita, at -20° and
 319 15° , and are up to more than three times larger com-
 320 pared to the aforementioned far-field value, whereas
 321 source positions in front of the nasal bone or along
 322 the process of the temporal bone show values closer
 323 to 10 cm. The closer the source to the skull, the more
 324 prominent the angular directionality of the apparent
 325 aperture. Hence, the maximum apparent aperture is
 326 more than three times larger than the skull diameter
 327 in the horizontal plane.

328 -3 dB widths are smaller than half a wavelength
 329 (super-resolution) throughout all azimuths at a dis-
 330 tance between source and skull of 5 cm, down to
 331 $\lambda_{min}/15$ (i.e. for $\varphi = -20^\circ$ and 15°). This shows that
 332 the skull-shaped antenna enables sub-wavelength fo-
 333 cusing of near-field sources and, furthermore, anatom-
 334 ical details of the skull may give rise to differences in
 335 resolution at certain positions due to the presence of
 336 evanescent waves. They can be described as a non-
 337 propagative spatial fluctuation field that decreases ex-
 338 ponentially over roughly one wavelength [10] and can

339 be created at a boundary between two media through
 340 certain incident angles of a propagating wave [15].
 341 Usually, their effect is not measured in the far field
 342 and the far-field diffraction law (Equation 4) does
 343 not account for such effects, limiting the resolution
 344 of time reversal. However, if near-field components of
 345 the wavefield are measured and incorporated in the
 346 time-reversal algorithm, subwavelength information,
 347 that is carried by evanescent waves, is incorporated
 348 in the time-reversal process, leading to super resolu-
 349 tion [23].

350 All these results are also approximately achieved
 351 via a one-sided evaluation of the signals, i.e. when
 352 only one receiver is used.

353 In summary, our data shows large variations in res-
 354 olution in the near-field, depending on the position
 355 of the source relative to the geometric complexities of
 356 the skull.

4 Conclusion

357
 358 In this study we measured elastic wave signals in a
 359 replica of a human skull due to an incident airborne
 360 sound emitted by a source at various distances and
 361 orientation with respect to the skull. Our goal was to
 362 investigate the physical limits of a sound-localization
 363 algorithm that uses full waveform information and the
 364 information contained in elastic waves propagating in
 365 the skull bone. While we do not at all claim to directly
 366 reproduce the sound localization "algorithm" that ex-
 367 ists in the human ear-brain system, our quantification
 368 of these limits may be considered as a point of com-
 369 parison in near-field psychoacoustics experiments.

370 We showed that the resolution of a time reversal
 371 scheme using a skull-shaped antenna with one or two
 372 receivers is consistent with the diffraction law in the
 373 far-field. The apparent apertures in the horizontal
 374 and sagittal planes are roughly consistent with the
 375 horizontal and vertical extent of the skull. Inter-
 376 estingly, the apparent aperture in the near-field is
 377 markedly increased (more than 3 times its value in
 378 the far-field) in the horizontal plane and at specific
 379 angles. In that case we can achieve super-resolution
 380 that may be associated to the non-negligible contri-
 381 bution of evanescent waves in the near-field.

382 Our results suggest that anatomical details of the
 383 skull give rise to complex features of the radiated
 384 sound field in the near-field, enabling sub-wavelength
 385 focusing and directional changes in resolution. We
 386 clearly find the influence of small anatomical geomet-
 387 ric complexities such as the orbital cavities to posi-
 388 tively influence resolution using elastic waves. We
 389 believe that it will be useful, in future studies, to ex-
 390 plore the performance of our algorithms in other fre-
 391 quency ranges and for other biological models (e.g.,
 392 echolocating species such as dolphins or bats).

393 As noted by Parseihian et al. [26], very few stud-
 394 ies in psychoacoustics have explored human sound lo-

395 calization performances for nearby sources (e.g. [6]).
 396 It appears to us that further experimental work is
 397 needed to more robustly evaluate how well humans
 398 localize nearby sources and if our findings can be re-
 399 lated to psychoacoustic studies in the near-field.

400 Acknowledgement

401 This project has received funding from the Euro-
 402 pean Union’s Horizon 2020 research and innovation
 403 programme under the Marie Skłodowska-Curie grant
 404 agreement No 641943 (ITN WAVES).

405 References

- 406 [1] Arthur H Benade. *Fundamentals of musical acoustics*.
 407 Courier Corporation, 1990.
- 408 [2] Simon Bernard, Quentin Grimal, and Pascal Laugier.
 409 Resonant ultrasound spectroscopy for viscoelastic
 410 characterization of anisotropic attenuative solid ma-
 411 terials. *The Journal of the Acoustical Society of*
 412 *America*, 135(5):2601–2613, 2014.
- 413 [3] Simon Bernard, Joannes Schneider, Peter Varga,
 414 Pascal Laugier, Kay Raum, and Quentin Grim-
 415 al. Elasticity–density and viscoelasticity–density
 416 relationships at the tibia mid-diaphysis assessed
 417 from resonant ultrasound spectroscopy measure-
 418 ments. *Biomechanics and modeling in mechanobiol-*
 419 *ogy*, 15(1):97–109, 2016.
- 420 [4] Eric Betzig, Jonathan Trautman, Tim Harris, Joseph
 421 Weiner, and Robert Kostelak. Breaking the diffraction
 422 barrier: optical microscopy on a nanometric
 423 scale. *Science*, 251(5000):1468, 1991.
- 424 [5] Peter Blomgren, George Papanicolaou, and Hongkai
 425 Zhao. Super-resolution in time-reversal acoustics.
 426 *The Journal of the Acoustical Society of America*,
 427 111(1):230–248, 2002.
- 428 [6] Douglas S Brungart, Nathaniel I Durlach, and
 429 William M Rabinowitz. Auditory localization of
 430 nearby sources. ii. localization of a broadband source.
 431 *The Journal of the Acoustical Society of America*,
 432 106(4):1956–1968, 1999.
- 433 [7] Stefan Catheline, Mathias Fink, Nicolas Quieffin, and
 434 Ros Kiri Ing. Acoustic source localization model us-
 435 ing in-skull reverberation and time reversal. *Applied*
 436 *physics letters*, 90(6):063902, 2007.
- 437 [8] Stephane G Conti, Philippe Roux, and William A
 438 Kuperman. Near-field time-reversal amplification.
 439 *The Journal of the Acoustical Society of America*,
 440 121(6):3602–3606, 2007.
- 441 [9] Julien de Rosny and Mathias Fink. Overcoming the
 442 diffraction limit in wave physics using a time-reversal
 443 mirror and a novel acoustic sink. *Physical review let-*
 444 *ters*, 89(12):124301, 2002.
- 445 [10] Julien de Rosny and Mathias Fink. Focusing prop-
 446 erties of near-field time reversal. *Physical Review A*,
 447 76(6):065801, 2007.
- [11] Arnaud Derode, Eric Larose, Mickael Tanter, Julien
 448 De Rosny, Arnaud Tourin, Michel Campillo, and
 449 Mathias Fink. Recovering the green’s function from
 450 field-field correlations in an open scattering medium
 451 (1). *The Journal of the Acoustical Society of America*,
 452 113(6):2973–2976, 2003.
- [12] Robert M Dickson, Andrew B Cubitt, Roger Y Tsien,
 454 and William E Moerner. On/off blinking and switch-
 455 ing behaviour of single molecules of green fluorescent
 456 protein. *Nature*, 388(6640):355–358, 1997.
- [13] Carsten Draeger and Mathias Fink. One-channel
 458 time-reversal in chaotic cavities: Theoretical limits.
 459 *The Journal of the Acoustical Society of America*,
 460 105(2):611–617, 1999.
- [14] Claudia Errico, Juliette Pierre, Sophie Pezet, Yann
 462 Desailly, Zsolt Lenkei, and Olivier Couture. Ultrafast
 463 ultrasound localization microscopy for deep super-
 464 resolution vascular imaging. *Nature*, 527(7579):499–
 465 508, 2015.
- [15] Mathias Fink. Time reversal of ultrasonic fields. i.
 467 basic principles. *IEEE transactions on ultrasonics,*
 468 *ferroelectrics, and frequency control*, 39(5):555–566,
 469 1992.
- [16] Mathias Fink. Time-reversed acoustics. *Scientific*
 471 *American*, 281(5):91–97, 1999.
- [17] Mathias Fink. Acoustic Time-Reversal Mirrors.
 473 *Imaging of Complex Media with Acoustic and Seis-*
 474 *mic Waves*, 17:17–43, 2001.
- [18] Mathias Fink. Time-reversal acoustics in complex
 476 environments. *Geophysics*, 71(4):SI151–SI164, 2006.
- [19] Bo Håkansson, Anders Brandt, Peder Carlsson, and
 478 Anders Tjellström. Resonance frequencies of the hu-
 479 man skull invivo. *The Journal of the Acoustical So-*
 480 *ciety of America*, 95(3):1474–1481, 1994.
- [20] Stefan W Hell and Jan Wichmann. Breaking
 482 the diffraction resolution limit by stimulated emis-
 483 sion: stimulated-emission-depletion fluorescence mi-
 484 croscopy. *Optics letters*, 19(11):780–782, 1994.
- [21] Shichao Hu, Jorge Trevino, Cesar Salvador, Shuichi
 486 Sakamoto, Junfeng Li, and Yōiti Suzuki. A local
 487 representation of the head-related transfer function.
 488 *The Journal of the Acoustical Society of America*,
 489 140(3):EL285–EL290, 2016.
- [22] Ros Kiri Ing, Nicolas Quieffin, Stefan Catheline, and
 491 Mathias Fink. In solid localization of finger impacts
 492 using acoustic time-reversal process. *Applied Physics*
 493 *Letters*, 87(20):204104, 2005.
- [23] Geoffroy Lerosey, Julien De Rosny, Arnaud Tourin,
 495 and Mathias Fink. Focusing beyond the diffraction
 496 limit with far-field time reversal. *Science*,
 497 315(5815):1120–1122, 2007.
- [24] Aaron Lewis, Michael Isaacson, Alec Harootunian,
 499 and A Muray. Development of a 500 Å spatial re-
 500 solution light microscope: I. light is efficiently trans-
 501 mitted through $\lambda/16$ diameter apertures. *Ultrami-*
 502 *croscopy*, 13(3):227–231, 1984.
- [25] Tom Littler, John J Knight, and PH Strange. Hearing
 504 by bone conduction and the use of bone-conduction
 505 hearing aids. *Proceedings of the Royal Society of*
 506 *Medicine*, 45(11):783, 1952.

- 508 [26] Gaëtan Parseihian, Christophe Jouffrais, and
509 Brian FG Katz. Reaching nearby sources: comparison
510 between real and virtual sound and visual targets.
511 *Frontiers in neuroscience*, 8, 2014.
- 512 [27] John Brian Pendry. Negative refraction makes a perfect
513 lens. *Physical review letters*, 85(18):3966, 2000.
- 514 [28] Dieter W Pohl, Winfried Denk, and Mark Lanz. Optical
515 stethoscopy: Image recording with resolution
516 $\lambda/20$. *Applied physics letters*, 44(7):651–653, 1984.
- 517 [29] Matthieu Rupin, Stefan Catheline, and Philippe
518 Roux. Super-resolution experiments on lamb waves
519 using a single emitter. *Applied Physics Letters*,
520 106(2):024103, 2015.
- 521 [30] F Simonetti. Localization of pointlike scatterers in
522 solids with subwavelength resolution. *Applied physics
523 letters*, 89(9):094105, 2006.
- 524 [31] Stefan Stenfelt. *Implantable Bone Conduction Hearing
525 Aids*, 71:10–21, 2011.
- 526 [32] Stefan Stenfelt and Richard L Goode. Bone-
527 conducted sound: physiological and clinical aspects.
528 *Otology & Neurotology*, 26(6):1245–1261, 2005.
- 529 [33] Chrysoula Tsogka and George C Papanicolaou. Time
530 reversal through a solid–liquid interface and super-
531 resolution. *Inverse problems*, 18(6):1639, 2002.
- 532 [34] John Van Opstal. *The auditory system and human
533 sound-localization behavior*. Academic Press, 2016.
- 534 [35] Bruce N Walker, Raymond M Stanley, Nandini Iyer,
535 Brian D Simpson, and Douglas S Brungart. Evaluation
536 of bone-conduction headsets for use in multi-
537 talker communication environments. *Proceedings of
538 the Human Factors and Ergonomics Society - 49th
539 Annual Meeting*, 49(17):1615–1619, 2005.
- 540 [36] Jack J Wazen, Jaclyn Spitzer, Soha N Ghossaini,
541 Ashutrosh Kacker, and Anne Zschommler. Results
542 of the bone-anchored hearing aid in unilateral hearing
543 loss. *The Laryngoscope*, 111(6):955–958, 2001.
- 544 [37] Elizabeth M Wenzel, Marianne Arruda, Doris J
545 Kistler, and Frederic L Wightman. Localization using
546 nonindividualized head-related transfer functions.
547 *The Journal of the Acoustical Society of America*,
548 94(1):111–123, 1993.